The Scientific Temper (2023) Vol. 14 (3): 834-839

E-ISSN: 2231-6396, ISSN: 0976-8653

Doi: 10.58414/SCIENTIFICTEMPER.2023.14.3.42

https://scientifictemper.com/

RESEARCH ARTICLE

# Synthesis and structural feasibility of photonic materials

**Y. Aboobucker Parvez[1], Prasanth Ponnusamy[2], Santhosh S[3], Rakhi Kamra[4]**

## Abstract

Based on the sample's texture and colour changed at various temperatures, this study examined the optical-thermal dependency of chiral nematic liquid crystal ink samples. This work examines ZnO thin films from an optical and structural standpoint. The required layer thickness was produced by spinning a zinc oxide solution over a cleaned glass substrate at 4000 rpm for 30 seconds at room temperature. The samples were then subjected to annealing, which was done from 150 to 600°C in increments of 50°C. This thin coating's optical characteristics were examined using an electron microscope and an ultraviolet-visible spectrophotometer. The optical transmittance, reflectance, and absorbance of zinc oxide were measured to estimate its optical band gap. When a light beam is transmitted or reflected, photonic crystals can display pertinent optical characteristics. The reflecting qualities in particular can be of interest in a two-dimensional photonic crystal and subsequently tuned for many technical applications, including selective high-reflection mirrors, photovoltaic solar systems, tuneable laser cavities, and many more. The development of Si has enabled the investigation of the reflective optical characteristics of two-dimensional photonic crystals grown on hybrid ZnO substrates with 10-45 nm size.

**Key words:** Photonic crystal, Sonication, Composite materials, ZnO-Si, Thermal annealing effects, and Photonic devices.

## Introduction

The capacity to manipulate the passage of photons in matter makes photonic crystals one of the most innovative and exciting achievements in the field of materials research. A photonic structure has the ability to function as a beam splitter, a selective transmitter/absorber of light, a wave guide, a light extractor in light emission diodes (LEDs), and, generally, a light processor in optical integrated circuits (D. Neelima Patnaik & Vardhani C.P. 2019). Undoubtedly, these and other innovative photonic crystal applications have the potential to replace or enhance some electronic device functions, and they do so with a number of important benefits, such as processing speeds that are on par with the speed of light in a vacuum (Edagawa K *et al*., 2008), (Pustai D. M *et al*., 2002). Among many other possible applications, photonic devices can be utilized in a variety of fields of interest, including telecommunications, for instance, in wavelength division multiplexing and modulation (Chaisakul P *et al*., 2014). Due to their ease of production using methods created for the electronics industry, such as chemical assisted ion beam etching (CAIBE), reactive ion etching (RIE), and more recent methods like focused ion beam milling (FIB), two-dimensional photonic crystals are of great interest (Smit M *et al*., 2012). We wish to show that we can modify the optical reflectance spectrum by inserting a variety of optical micro-cavities within the photonic construction. Another explanation for the high optical reflectance is a two-dimensional photonic crystal with a collection of micro-optical cavities. To put it another way, it is suggested in this study that optical micro-cavity arrays be used to create a strong wave coupling in a photonic structure that can improve its reflective qualities at the chosen wavelength. The implications of adding an optical cavity or two to photonic crystals have previously been investigated in research papers that have been published in the literature. These cavities or defects are often characterized by a linear section of these flaws and a point defector, which together form a waveguide (Abe H *et al*., 2015). There are oscillation modes that have been developed in the cavity that display

[1]Department of Mechanical Engineering, SNS College of Technology, Coimbatore, Tamil Nadu, India.

[2]Department of Mechanical Engineering, Tagore Institute of Engineering and Technology, Salem, Tamil Nadu, India.

[3]Department of Mechanical Engineering, Sri Krishna College of Technology, Coimbatore, Tamil Nadu, India.

[4]Department of Electrical and Electronics Engineering, Maharaja Surajmal Institute of Technology, Janakpuri, New Delhi, Delhi, India.

***Corresponding Author:** Y. Aboobucker Parvez, Department of Mechanical Engineering, SNS College of Technology, Coimbatore, Tamil Nadu, India, E-Mail: aboobucker.sns@gmail.com

**How to cite this article:** Parvez, Y.A., Ponnusamy, P., Santhosh, S., Kamra, R. (2023). Synthesis and structural feasibility of photonic materials. The Scientific Temper, **14**(3): 834-839.

Doi: 10.58414/SCIENTIFICTEMPER.2023.14.3.42

**Source of support:** Nil

**Conflict of interest:** None.



**Received:** 13/07/2023 **Accepted:** 10/08/2023 **Published** : 25/09/2023

highly nonlinear wave resonance effects. Additionally, wave coupling has been noted as a result of the interplay between the recognized oscillation modes with structural flaws that disrupt the periodicity of the holes in the photonic crystal, which is typically a triangular lattice (Hennessy K *et al*., (007).

### *Literature review*

Spin-coating was utilized to deposit ZnO on a glass substrate because it is simple to cover large areas and can be processed at low temperatures. It may also be used to create uniformly composed porous oxide films with many components (S. Sanjeev & D. Kekuda. 2015). In traditional spin-coating methods, the spin-coater was spun up, the program was set up, liquid was dispensed, and the program was performed in ambient circumstances at room temperature (S. Yusan *et al*., 2016). ZNO solution may be spin-coated over a previously cleaned glass substrate for 30 seconds at 4000 rpm (K. G. Kanade *et al*., 2006). The film's thickness must be achieved by a succession of coating and drying cycles. Because of its slow rate of evaporation and lack of apparent absorption or emission (ZnO), dissolving zinc oxide in ethanol is achievable. A combination of ZnO powder and ethanol must be sonicated for three hours in order to do this (M. Sabbaghan *et al*., 2012). An ASPEX 3020 scanning electron microscope (SEM) and an Avantes Avalight-DH-5-BAL UV/V is spectrophotometer are used to help it comprehend the optical characteristics of ZnO thin films. ZnO serves as an essential semiconductor in organic electronics and is utilized in many different applications, including solar cells and optoelectronics. On a glass substrate, ZnO can be coated by spray pyrolysis, thermal vacuum deposition, sputtering, or spin coating, for example.(E. Darezereshki *et al*., 2011), (H. Wang*et al*., 2013). Zinc oxide can be used in solar cells as an electron transport layer since it is a low-cost n-type semiconductor with great thermal and mechanical stability at ambient temperature. It is very photo-stable and has a wide range of ray absorption capabilities. ZnO is a commonly used heterogeneous catalyst and essential N-type semiconductor. It is cheap, nontoxic, insoluble, and has good catalytic activity (A. Kołodziejczak- Radzimska & T. Jesionowski. 2014). ZnO is a particularly significant material since it also has a number of other characteristics, such as a wide-bandgap semiconductor with a high excitation binding energy of 60 MeV. There is a lot of interest in ZnO since it is a commonly accessible and affordable substrate layer for electrical processes like solar cells and flat panel displays (C. C. Chen *et al*., 2008).

### *Experimental Details*

In the initial phase of this study, numerical simulations of the optical characteristics of two PhCs were carried out using both custom software created by our research team based on the finite element method and commercial software such as Comsol Multiphysics ( Klinton Davis *et al*., 2019).

The experimental production of the 2D triangular lattice photonic crystal structure using ZnO sheets. In Figure 1, ZnO is conceptually represented as a B(n)/ZnO/c-Si(p) hetero-junction. Starting out, the plasma enhanced MOCVD technique is used to create ZnO films on c-plane sapphire substrates that range in thickness from 10 to 45 nm. According to the defined region of the film's electron diffraction pattern, single crystalline ZnO is created along the c-axis. The films are then etched with triangular latticed arrays of cylindrical air columns by a focused Ga3+ ion beam that has been accelerated to 30 KeV and 30 pA current. Focused ion beam (FIB), a method that has been extensively utilized for mask-free and resistless nano-scale patterning, enables precise control of the position, size, and density of the air cylinders in the ZnO films. Due to the tiny hole size (r 30nm) and technical restrictions of the etching apparatus, some deviation from perfect periodic patterns cannot be avoided. The SEM image of one of our typical PhCS samples in Figure makes it very evident. The apparent non-roundness of the air holes is due to sample drifting during etching and the facility resolution limit. A little bit smaller and very close to vertical is the bottom radius of the side wall of air holes, which is not seen here. Due to the etching, which produces etched patterns that are generally 8 x 8 m in size, the photonic layer is somewhat thinner than the film in locations that are not patterned. The bombardment of Ga ions during the FIB etching process severely degrades the ZnO's crystalline quality, and the patterned region's photoluminescence emission is significantly lower than that of the unpatterned area. In order to repair this damage, we found that annealing the patterned films in oxygen for an hour at 600°C partly restores the emission.

## Material and Methods

ZnO powder and glass slides were supplied by Sigma-Aldrich for use in this investigation.

### *ZnO Sample Solution Preparation*

The ZnO powder, 10 to 45 nm, was obtained from Sigma Aldrich and mixed with an ethanol solution. The

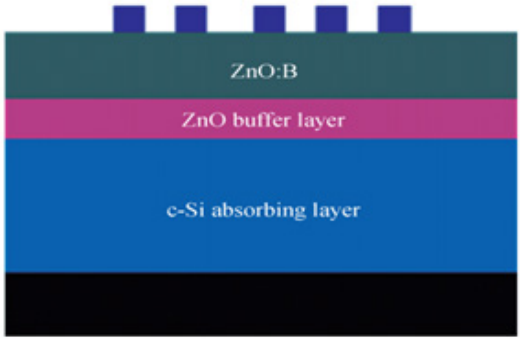


**Figure 1:** Schematic structure of ZnO:B(n)/ZnO/c-Si(p) Heterojunction input parameters used in the present simulation

**Table 1:** Parameters used in the simulation [https://pubs.rsc.org/2019]

| *Parameter* | *ZnO* | *Si* |
|---|---|---|
| Thickness/nm | 10–45 | 1 *$10^5$–3* $10^5$ |
| Dielectric Constant | 7.8 | 11.9 |
| Electron affinity (eV) | 4.5 | 4.05 |
| Band Gap (eV) | 3.37 | 1.12 |
| Effective Conduction band density ($cm^3$) | 2:2 * $10^{18}$ | 2. 8 * $10^{19}$ |
| Effective Valence band density ($cm^3$) | 1.8*$10^{19}$ | 1.04 *$10^{19}$ |
| Electron Mobility ($cm^2 V^{-1} s^{-1}$) | 5 | 1040 |
| Hole Mobility ($cm^2 V^{-1} s^{-1}$) | 1 | 412 |
| Acceptor concentration ($cm^{-3}$) | 0 | 1*$10^{16}$ |
| Donor concentration ($cm^{-3}$) | 1.7*$10^{17}$ | 0 |
| Thermal velocity of electron (cm/s) | 1.*$10^{17}$ | 1.*$10^{17}$ |
| Thermal velocity of holes (cm/s) | 1.*$10^{17}$ | 1.*$10^{17}$ |
| Layer density ($g/cm^{-3}$) | 5.606 | 2.328 |

homogenous mixture and ZnO powder were totally dissolved in the solution after three hours of sonication at room temperature without heating. It was decided to utilize ethanol as a solvent since it doesn't absorb or emit light in the visible spectrum.

### *Substrate Preparation*

The substrates for this experiment were glass slides with a dimension of 25.4 by 76.2 mm. The substrates underwent a second round of washing and an ultrasonically-assisted 15 minute 30°C rinse before being put to use. Following a blow-drying procedure in a nitrogen atmosphere, an ultrasonic bath at 30°C for 15 minutes was used to remove the isopropanol acid [IPA].

### *Deposition of ZNO on the substrate using spin-Coater*

To serve as a delivery point for a solution, a pre-cleaned substrate was mounted on a spin-coater stub, model WS-650MZ-23NPP. After the program has been run and the solution has been applied, the substrate has been given a brief window of time to absorb it. ZnO solution was spin coated on a glass substrate for 30 seconds at 4000 rpm while it was still warm to the touch to create a layer that was 35 nm thick. To achieve the necessary film thickness, many cycles of coating and drying are needed. Spreading the liquid occurs at low rotational speeds, whereas moisture removal occurs at high rotational speeds. Its lower cost and shorter implementation time are two benefits of this approach. The samples are heated to 150°C for an hour, after which all non-ZnO components are removed, and the samples are then gently cooled to room temperature. The PLD system was vacuumed to 1.210 to 4 Pa (99.999%), and then high quality oxygen at a pressure of 0.13 Pa was fed into it. The ZnO target was abraded by a focused pulse laser beam while the substrate was heated to 600°C through an optical window in the system chamber. After the 15 minute deposition, this sample of ZnO/Si material was made. We employed the JCK-500A RF magnetron sputtering apparatus, which sputtered GaN target onto a ZnO buffer layer, to produce thin GaN films. The target made of sintered GaN is pure to 99.999%. 3.210 to 4 Pa served as the system's vacuum. The system was run on high-purity argon gas at a partial pressure of 2 Pa. The sample was sputtered with 150 watts of electricity over the course of 90 minutes.

### *Samples Characterization*

4 Srw 21-501042 The furnace was a carbolite tube. The preheated samples were annealed for 60 minutes in increments of 50°C at temperatures ranging from 150 to 600°C, and then they were cooled in argon gas to room temperature. The control sample was left untreated. The word "annealing" describes the procedure of heating a material over its critical temperature, keeping it there, and then quickly cooling it. This approach allows for the improvement of cold working qualities, ductility enhancement, material softening, internal stress relief, and ductility. (Sunday Wilson Balogun *et al*., 2017).

## Results and Discussions

A scanning electron microscope (SEM) was used to get pictures of the materials' surfaces. All of the samples had to be cut to the appropriate size in order to fit the specimen stub of the SEM.

### *Morphological Characterization*

At different magnifications, SEM is a useful technique for analyzing the surface morphology of materials. to investigate the sample's surface behaviour. The SEM morphology of the samples was investigated. Figure, which illustrates the sample at temperatures of 150, 350, and 500°C, displays the surface morphologies of samples cooked to various degrees. The morphology of the samples changes from Figures 2 to 4 depending on the annealing temperature. The surface was seen to be rougher the higher the annealing temperature. It's probable that an increase in grain size results from raising the annealing temperature when these morphological pictures occur.

Increases in photon energy absorption are associated with rising annealing temperatures. Furthermore, it shows that transmission grows with increasing wavelength and decreases with increasing annealing temperature, respectively. Thin zinc oxide coatings were created on a glass substrate by annealing it at temperatures between 150 and 600°C in increments of 50°C. The absorbance rose with higher annealing temperatures, but it dropped when wavelengths were raised. The research demonstrates that the morphological and optical properties of ZnO thin films are affected by the annealing temperature. The transmission spectra of the films were assessed with a UV-vis spectrophotometer. Visible spectrum transparency is quite

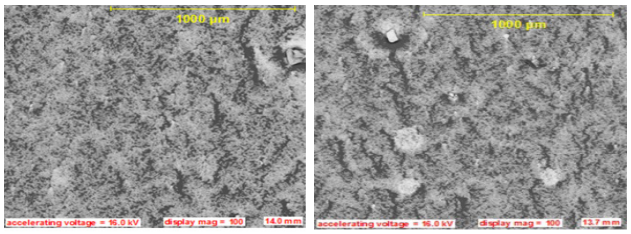

**Figure 2:** (a) SEM image of ZNO-with Si film annealed at 150°C (b) 200°C

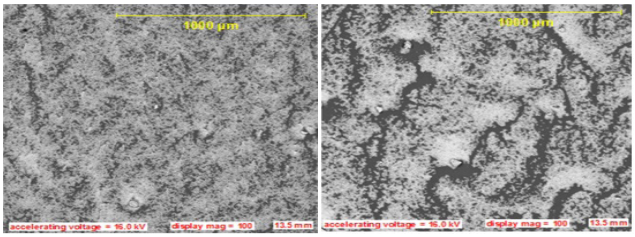

**Figure 3:** (a) SEM image of ZNO with-Si film annealed at 300°C (b) 400°C

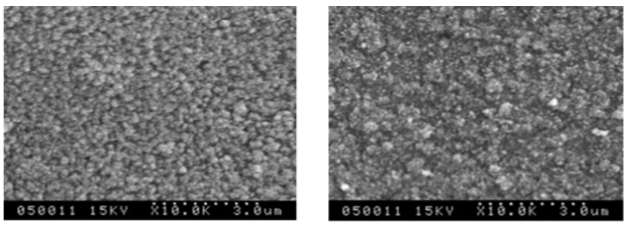

**Figure 4:** (a)SEM image of ZNO film annealed at 500°C (b) 600°C

high for the films. Extinction coefficients, however, have been developed. As the annealing temperature rose, the extinction coefficient of ZnO films changed a little. Here is a preliminary estimate of the bandgap value for bulk ZnO. The band gap is reduced as annealing temperature is raised. As annealing temperature rises, surface roughness of the samples increases as grain size grows and Eg decreases as a result.

### *Numerical Simulations*

Numerous astounding conclusions concerning the optical characteristics of each PhC under consideration were reached from the numerical computations made in this study. The spectrum optical reflectance of the photonic crystal comprising the array of optical cavities first revealed an odd behaviour. The optical reflectance computed for the two photonic crystals examined in this study is shown in Figure 5(c). The measurement for the control sample PhC1 is represented by a dashed line, whereas the measurement for sample PhC2, which has a variety of optical cavities, is represented by a solid black line. For instance, as seen in Figure 5b.

### *Photonic Band Calculation*

The calculations of the photonic bands structure of both the examined materials were done using numerical simulations.

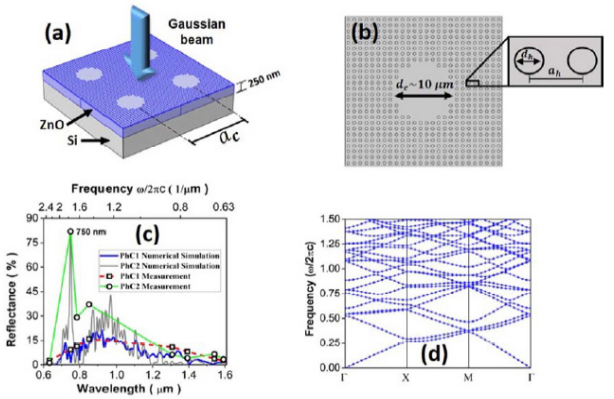


**Figure 5:** (a) Schematic diagram of the structural parameters of a section of the photonic crystal PhC2 considered in numerical simulations, (b) a section of the PhC2 showing the holes diameter, and the lattice constant of the square array of air-filled holes, and the diameter of one of the optical cavities. (c) Calculated optical reflectance for the control sample PhC1 represented by a dashed line, and the test sample PhC2 denoted by a continuous solid black line, respectively. The squares and the dots represent the experimental measurements for the PhC1 and PhC2, respectively, which have been joined by a dashed blue line and a solid green line, respectively, for eye guidance only. (d) Analysis of the control sample's photonic band structure using numerical simulations One-layer ZnO-Si substrate is machined to form a regular square lattice of holes filled with air for PhC1.

It was presumed that periodic boundary conditions (PBC) would be used to account for the periodicity of the structural factors defining each PhC under study. The SEM images of the PhC1 and PhC2 samples are shown in Figures 6a and b, respectively. Calculation of the stimulated emission generation rate in silicon as a function of the incoming radiation's wavelength is shown in Figure 6c in units of 1/(m3s).

The reason for this is that it was discovered that the PhC2 sample has a significant number of photonic bands, which effectively make up an endless series of propagation frequencies that are permitted beyond the frequency of 0.09 w/2 c. It is amazing to see in Figure that the computed photonic band structure for the PhC1 sample does not show any full photonic band gap around the normalized frequency corresponding to the wavelength range where the optical reflectance exhibited an increase. For the relevant frequency ranges in the structures of both photonic bands, to the sample PhC2. In fact, it is logical to anticipate that the PhC2 sample's photonic band structure will largely resemble the PhC1 sample's photonic band structure. A large number of permissible states are introduced into the frequency domain by the cavities array included in PhC2, though. This is because the optical cavities in the PhC2 sample are continuous thin film regions without any air holes that result in a significant number of permitted bands below the frequency range of 1.32 to 1.36 w/2c in the photonic band structure.

The following are the primary causes for the improvement in the antibacterial activity of manufactured nanoparticles:

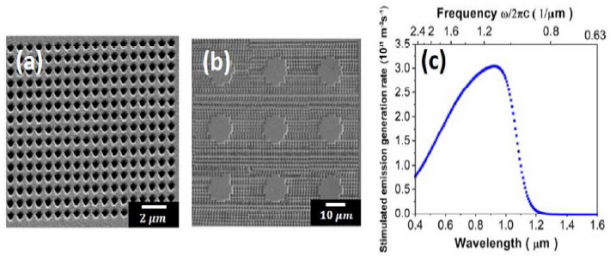


**Figure 6:** (a) and (b) scanning electron microscope (SEM) micrographs of the PhC1 and the PhC2 samples, respectively. (c) Calculation of the stimulated emission generation rate in units of 1/(m3s) as a function of the wavelength of incident radiation in silicon

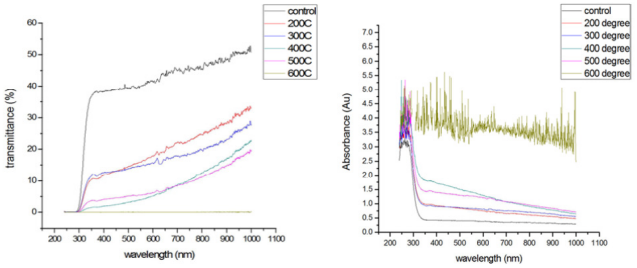


**Figure 7:** (a)Transmittance versus wavelength graph for selected temperatures. (b) Absorbance

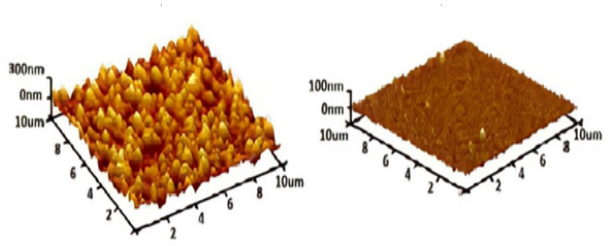


**Figure 8:** Surface morphology of ZnO-Si

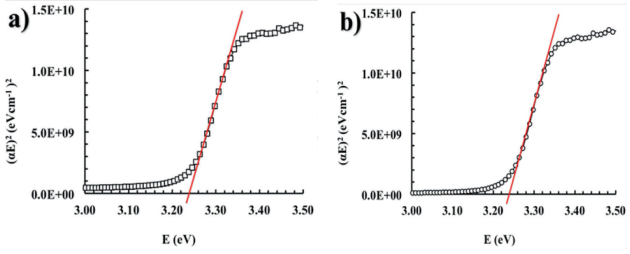


**Figure 9:** Optimal band gap ZnO for all samples

The crystallite's size was decreased, $Zn^2$ ions were released, and reactive oxygen species (ROS) were produced, among other effects. Because the particles are tiny, they can penetrate the bacteria's inside and interact with it, which may cause cell membranes to break, cellular contents to spill out, and consequent cell death. The development of free carriers in the system, which results in the substitution of the $Co^2$ ions in the $Zn^2$ sites in the ZnO lattice, is what leads to an increase in the production of ROS. Reactive oxygen substances (ROS) can be generated by these free carriers. Figure 7: a & b shows the Transmittance versus wavelength graph for selected temperatures.

The optical band gap for the nanoparticles ranged from 3.33 to 3.41 eV based on the UV on-set, which was much higher than the optical band gap for nanorods made in a DMF solvent solution, which ranged from 3.1 to 3.24 eV. Due to the varied solvents used during their manufacture, ZnO nanorods had maximum absorption maxima ranging from 3.30 to 3.39 eV, with acetonitrile producing nanorods with the lowest optical band gap at 3.10 eV. ZnO nanorods formed in xylene and toluene have an optical band gap of 3.20 eV 0.04, whereas those made in toluene have a band gap of 3.22 eV 0.010. Because of its crystallinity, crystal growth facets, and grain size, all of which are changes in the optical band gaps, the nanostructured ZnO, which is shown in Figure 9 a&b, has a smaller effective band gap than its bulk value of 3.37 eV. According to various authors, these postulates simplify the mathematical equations that are employed to describe the optical characteristics of the layer of material under study. Therefore, just the measurement of TD and RD were required for the current situation. Because diffuse components predominate, it is noteworthy that the values of TD and RD nearly approximate the values of T and R utilized in M1 and M2.

## Conclusion

We looked at the form and optical characteristics of zinc oxide thin films under various heating scenarios. While heating zinc oxide, the greatest visible spectrum photon absorption occurred at 500°C. Zinc oxide has the greatest extinction coefficient in the visible spectrum at 500°C. The band gap energy decreases with temperature, decreasing from 4.03 to 3.5 eV. On a glass substrate that has been heated over its melting point, zinc oxide temporarily changes how much photon energy it absorbs. The shortcomings necessitate annealing at a temperature greater than 500°C. It was discovered that surface roughness rises with zinc oxide thick film annealing temperature using an ASPEX 3020 SEM. It is common knowledge that as the heating temperature increases, zinc oxide transmission diminishes. ZnO films are suitable for use as buffer layers in solar cells because of their optical stability between 400 and 700 nm. The waveform of photon absorption at 600°C is different and is comparable to those that have been annealed at lower temperatures. When annealed at lower temperatures, the extinction coefficient of zinc thin films grows more gradually and linearly; but, when annealed over 600°C, it becomes more volatile and changeable than under other conditions.

## References

Kołodziejczak- Radzimska, T. Jesionowski. Zinc OxideFrom Synthesis to Application: A Review. Materials. v. 7, pp. 2833-2881.

Abe H., Narimatsu M., Watanabe T., Furumoto T., YokouchiY., Nishijima Y., Kita S., Tomitaka A., Ota S, Takemura Y., & Baba T. (2015). Living-cell imaging using a photonic crystal nano

laser array. Optics Express, v. 23, n. 13, pp. 17056.

C. Chen, P. Liu, C. H Lu. (2008). Synthesis and Characterization of nano-sized ZnO powders by direct precipitation method. Chem Eng J. v. 144, pp. 509–513.

Chaisakul P., Marris-Morini D., Frigerio J., Chrastina D. Rouifed M.-S., Cecchi S., Crozat P., Isella G., & Vivien L. (2014). Integrated germanium optical interconnects on silicon substrates. Nature Photonics, v. 8, n. 6, pp. 482-488.

Neelima Patnaik, Vardhani C.P (2019). A Comparative Study of Litao3 Y-Branch Symmetric and Asymmetric Optical Power Splitter with S-Bend Waveguides with Various Parameters,IJITEE, v. 8, n.8, pp. 3280-3282.

Darezereshki, M. Alizadeh, F. Bakhtiari, M. Schaffie. (2011). A novel thermal decomposition method for the synthesis of ZnO nanoparticles from low concentration ZnSO4 solutions. Appl Clay Sci. v. 54, pp. 107-111.

Edagawa K., Kanoko S., & Notomi M. (2008). Photonic Amorphous Diamond Structure with a 3D Photonic Band Gap. Physical Review Letters, v. 100, n. 1, pp. 013901

H. Wang, C. Li, H. Zhao, R Li, J. Liu. (2014). Synthesis, characterization, and electrical conductivity of ZnO with different morphologies. Powder Technol. 2013; 239: 266-271.

Hennessy K., Badolato A., Winger M., Gerace D., Atatüre M., Gulde S., Fält S., Hu E. L., & Imamoğlu A. (2007). Quantum nature of a strongly coupled single quantum dot-cavity system. Nature, v. 445, pp. 896–899

https://pubs.rsc.org/en/content/articlelanding/2019/ra/c9ra02091h

K. G. Kanade, B. B. Kale, R. C. Aiyer, B. K. (2006). Das Effect of solvents on the synthesis of nano-size zinc oxide and its properties. Mater Res Bull. v. 41, pp. 590-600.

Kita S., Nozaki K., & Baba T. (2008). Refractive index sensing utilizing a cw photonic crystal nanolaser and its array configuration. Optic Express, v. 16, n. 11, pp. 8174.

Klinton Davis, Ryan Yarbrough, Michael Froeschle, Jamel White, and Hemali Rathnayake. (2019) Band gap engineered zinc oxide nanostructures *via* a sol–gel synthesis of solvent driven shape-controlled crystal growth, RSC Adv. v. 9, n. 26. doi: 10.1039/c9ra02091h

M. Sabbaghan, A. S Shahvelayati, S. E Bashtani. (2012). Synthesis and optical properties of ZnO nanostructures in imidazoliumbased ionic liquids. Solid State Sci. v. 14, pp. 1191-1195.

Notomi M. (2010). Manipulating light with strongly modulated photonic crystals. Reports on Progress in Physics, v. 73, n. 9, pp. 096501.

Pustai D. M., Sharkawy A., Shi S., & Prather D. W. (2002). Tunable photonic crystal microcavities. Applied Optics, v. 41, n. 26, pp. 5574.

S. Sanjeev, D. Kekuda. (2015). Effect of Annealing Temperature on the Structural and Optical Properties of Zinc Oxide (ZnO) Thin Films Prepared by Spin Coating Process IOP Conf. Ser.: Mater. Sci. Eng. v. 73, pp. 012149.

S. Yusan, A. Bampaiti, S. Aytas, S. Erenturk, M. A. A Aslani. (2016). Synthesis and structural properties of ZnO and diatomitesupported ZnO nanostructures. Ceram Int. v. 42 pp. 2158– 2163.

Smit M., Van der Tol J., & Hill M. (2012). Moore's law in photonics. Laser & Photonics Reviews, v. 6, n. 1, pp. 1-13.

Sunday Wilson Balogun, Yekini Kolawole Sanusi, Adebayo Olaniyi Aina. (2017) Impact of Post- Deposition Heat Treatment on the Morphology and Optical Properties of Zinc Oxide (ZnO) Thin Film Prepared by Spin-Coating Technique, *Journal of Photonic Materials and Technology*. v. 3, n. 3, pp. 20-28. doi: 10.11648/j.jmpt.20170303.11